FULL PAPER

On-the-Spot Immobilization of Quantum Dots, Graphene Oxide, and Proteins via Hydrophobins

*Alfredo M. Gravagnuolo, Eden Morales-Narváez, Charlene Regina Santos Matos, Sara Longobardi, Paola Giardina, and Arben Merkoçi**

Class I hydrophobin Vmh2, a peculiar surface active and versatile fungal protein, is known to self-assemble into chemically stable amphiphilic films, to be able to change wettability of surfaces, and to strongly adsorb other proteins. Herein, a fast, highly homogeneous and efficient glass functionalization by spontaneous self-assembling of Vmh2 at liquid–solid interfaces is achieved (in 2 min). The Vmh2-coated glass slides are proven to immobilize not only proteins but also nanomaterials such as graphene oxide (GO) and quantum dots (QDs). As models, bovine serum albumin labeled with Alexa 555 fluorophore, anti-immunoglobulin G antibodies, and cadmium telluride QDs are patterned in a microarray fashion in order to demonstrate functionality, reproducibility, and versatility of the proposed substrate. Additionally, a GO layer is effectively and homogeneously self-assembled onto the studied functionalized surface. This approach offers a quick and simple alternative to immobilize nanomaterials and proteins, which is appealing for new bioanalytical and nanobioenabled applications.

1. Introduction

Surface modification at the molecular level is a paramount method enabling functional properties in substrates with interest for biotechnological applications.[1] Nanosized materials revealing new fascinating properties (neither displayed by the bulk materials nor by the discrete molecules) and very high surface-area-to-volume ratio are progressively being integrated in the next-generation biomolecular devices in several fields such as nanomedicine, (bio)analytical chemistry, and bioelectronics.[2,3]

Graphene oxide (GO) and semiconductor (III–V and II–VI) quantum dots (QDs) are two of the most studied optically active nanomaterials exhibiting extraordinary nanoscale properties. QDs are also known as colloidal luminescent semiconductor nanocrystals, generally measuring 1–10 nm. Their optical properties have been reported to be advantageous when compared with those of conventional organic dyes for biomedical applications.[4–7] For instance, QDs bear size-dependent emission, from UV to mid-IR region,[8] broad excitation wavelength, large Stokes' shift, symmetric and narrow emission spectra, high brightness, and they do not display photobleaching phenomenon.[9] As a consequence, QDs provide versatile tools for optical or electrical multiplexing (detection of multiple signals, spectrally, spatially, or temporally resolved),[6,10–12] long-term and single molecule imaging,[13,14] and offer novel approaches in biotechnology,[15] based on bar-coding,[16] chemical noses,[17] logic-gate operations, and optical switches[18] among others.

GO is a 2D nanomaterial belonging to the family of carbon allotropes[19,20] characterized by heterogeneous chemical structure and a very large surface area, e.g., 737 m^2 g^{-1}.[21] As a highly oxidized derivate of graphite, it is easily processed in aqueous solutions[22–25] and synthesized in large quantity,[20,26] and it is applied in several biotechnological platforms.[27]

The GO monolayer is also a high tunable nanomaterial given the lateral size[28] and the oxidation degree,[29] which are pivotal marks of the 2D carbon structure.[30] Indeed, it can be photoluminescent over a broad range of wavelengths, from UV to near-IR;[31] a universal long-range superquencher;[32–35] capable of direct binding/wiring with biomolecules;[2,36] and modulated to interact with living cells in specific ways.[37] Interestingly, it shows higher quenching efficiency of QDs' photoluminescence when compared with other 1D or 3D carbon structures.[38] The advantageous properties of GO have been pointed up in optical detection,[39,40] also in this case enabling applications of advanced concepts in sensing such as real-time intracellular tracking[41,42] (even enhanced using nanomotors),[43] drug discovery,[44] logic-gates,[45] and nose-like platforms.[28,46]

QDs being vigorous donors and GO sheets being powerful energy transfer acceptors, the interplay of these two complementary nanomaterials in rationally designed biological assemblies can open the avenue to unparalleled performances in sensing creating opportunities for the development of low-cost

Dr. A. M. Gravagnuolo, Dr. E. Morales-Narváez, C. R. S. Matos, Prof. A. Merkoçi
ICN2–Catalan Institute of Nanoscience and Nanotechnology
08193 Barcelona, Spain
E-mail: arben.merkoci@icn.cat
Dr. A. M. Gravagnuolo, Dr. S. Longobardi, Prof. P. Giardina
Department of Chemical Sciences
University of Naples "Federico II,"
80126 Naples, Italy
Prof. A. Merkoçi
ICREA–Catalan Institution for Research and Advanced Studies
08010 Barcelona, Spain

DOI: 10.1002/adfm.201502837

and rapid molecular diagnostics tools,[47–49] possibly reaching digital-like responses.[50,51]

Additionally, new dimensions for the elaboration of novel (bio)sensors based on diverse mechanisms of transduction can be created through immobilization of the molecular species on chips with high spatial resolution, using GO as a donor[52] or an acceptor[53] of FRET, QDs,[54], or a combination of them.[50] Immobilization is a crucial step to design labs-on-a-surface for multiplex-screening, high-throughput sensing, real-time detection, device miniaturization, and reduction of reagent amount.[55,56] The disposition of concentrated sensing molecular assemblies in submicrometric sectors, light stimulated by focalized radiation, also allows the signal-to-noise ratio and sensitivity to bump up, therefore reaching very low detection limits.[53,54,57]

However, efficient integration of nanomaterials and proteins in functional devices requires strategies to control their assemblies, without hampering their properties, enhancing the features of the base building blocks.[58,59]

Self-assembling of proteins, nonsynthetic "nanomachines" endowed with a broad variety of functions, is nowadays intensively studied as a fundamental and green strategy to build hierarchical structures in both living systems and hybrid functional assemblies for bio-nanotechnological purposes.[60,61] Hydrophobins (HFB) are self-assembling proteins commonly produced by filamentous fungi that, arising from the typical fungal life style, have evolved "Janus-faced" structures[62] and special functions.[63] Indeed, superior fungi live their life cycles facing the liquid–air and liquid–solid interfaces, escaping from wet environment by lowering the surface tension of water using soluble hydrophobins and by coating their body with hydrophobic, stable protein layers. In their soluble forms, HFBs are excellent surface active proteins[64] and find applications in industrial and medical biotechnology as foams, emulsions, and dispersions stabilizers. HFBs also self-assemble into amphiphilic structured layers able to reverse the wettability of both hydrophilic and hydrophobic materials.[65] Since the layers formed by HFBs of Class I show exceptional chemical stability, i.e., in 3 M NaOH or 3 M HCl,[66] or in hot water in the presence of detergents (sodium dodecyl sulfate, SDS),[67] they find applications in the biofunctionalization of the surfaces. Moreover, the adhesive properties of the HFB films, exploited by fungi to grow on hydrophobic surfaces, have been demonstrated to be effective as a "primer" for surfaces bioconjugation of another protein layer on inert surfaces.[68]

Vmh2 from the white-rot fungus *Pleurotus ostreatus* is one of the most hydrophobic HFBs known, soluble in low polar solvents. This Class I HFB has been isolated and studied in our laboratories and used for modification of steel,[69,70] nanostructured silicon,[67] and graphene-based materials.[71] The nanometric layer (≈2.5 nm tick) of Vmh2 has been characterized on different surfaces as well its self-assembled rod-like structures, typically formed by Class I HFBs.[72] The Vmh2 monolayer acts as a bioactive substrate to bind other proteins, which show improved stability and activity when bound on the biohybrid chips.[70–73]

In this work, we propose a fast, highly homogeneous, and efficient glass functionalization method by spontaneous self-assembling of Vmh2 at liquid–solid interface. In addition, we demonstrate for the first time the immobilization of nanomaterials and proteins via hydrophobins in a microarray fashion, which results to be a time-saving process. Relevant surface characteristics of biofunctionalized slides are evaluated and compared with a commercially available, standard aminosilane substrate. Micropatterning immobilization of labeled proteins and cadmium telluride (CdTe) QDs is performed obtaining high signal-to-background ratio. Moreover, a GO layer is assembled on the Vmh2 substrate. Functionality of proteins on Vmh2 layer is shown using an immunoassay in a microarray format.[7]

2. Results and Discussion

2.1. Functionalization of Glass by Self-Assembling Layers of Vmh2

Immobilization of proteins and nanomaterials on glass was performed in three steps (**Figure 1**): (1) preparation of negatively charged glass surfaces by air plasma treatment (Figure 1A); (2) quick assembly of amphiphilic layers of Vmh2 by the dip casting method (Figure 1B1); (3) simple immobilization of proteins (Figure 1B) and nanomaterials (Figure 1C) on the Vmh2 substrate by microarray patterning or dip casting.

First, the use of highly homogeneous and chemically controlled substrates is essential to develop standard procedures for surface adhesion of molecular layers.[74] Air plasma can be used in surface technology to process glasses, highly oxidizing

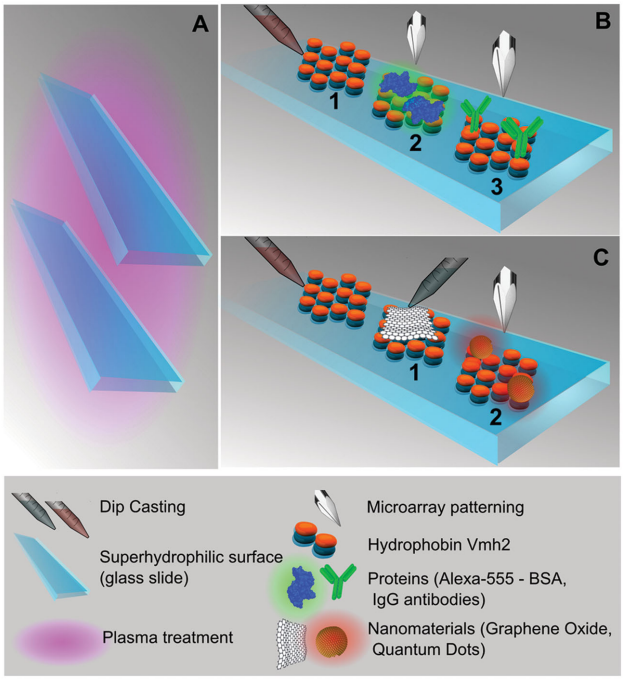

Figure 1. General procedure for hydrophobin Vmh2-based glass slide functionalization (schematic representation, not to scale). A) 2 min plasma treatment of bare glass slides. B) Biofunctionalization of a glass slide with B1) Vmh2 layer by dip casting, B2) Alexa555–BSA by microarray patterning, and B3) anti-IgG antibodies by microarray patterning. C) Immobilization of nanomaterials with C1) graphene oxide by manual dip coating and C2) CdTe quantum dots by microarray patterning.

a few monolayers of the surface and removing organic contaminants. Since Vmh2 in 60% ethanol solution is endowed with positive electrostatic potential (measured by electrophoretic mobility),[71] negatively charged glass surfaces obtained by air plasma treatment were appropriate to enhance the studied protein binding. Moreover, given that the adhesion energy of the protein layer is dominated by hydrophobic and Coulombic charge interactions,[75,76] the hydrophobin orientation will determine the efficiency of immobilization of the interested molecules to the modified surface.

Precleaned glass slides (provided by two manufacturers), MI and MII, showed a water contact angle (WCA) of 18° ± 3° and 31° ± 3° (mean ± standard deviation), respectively. Following 2 min of plasma treatment, MI and MII were not distinguishable by WCA analysis, showing a very homogeneous superhydrophilic surface (WCA, <5°).

Second, the high wettable treated glass and the low surface tension of the Vmh2 solvent (60% ethanol) allowed a thin liquid layer to be readily formed onto the whole top area of the slides, 18.8 cm^2, upon casting 200 µL of 0–400 ng $µL^{-1}$ Vmh2 solutions. After only 2 min of incubation at room temperature, the excess of Vmh2 was washed out by 60% ethanol and the surface was dried in a stream of nitrogen. The analysis of the WCA showed a shift of ≈60° upon quick assembly of Vmh2 saturating the surface by 100 ng $µL^{-1}$ Vmh2 (see **Figure 2**).

However, ≈80% of contact angle shift, 48° ± 2°, was reached using only 25 ng $µL^{-1}$ Vmh2, corresponding to 270 ng cm^{-2} of glass area. On the basis of the diameter of a globular monomer of hydrophobin, ≈25 Å,[77] (also equal to the thickness of a Vmh2 monolayer measured by atomic force microscopy (AFM))[72] and of the molecular weight of Vmh2, 8563 Da,[78] the estimated amount of Vmh2 required to form an ideal monolayer is about 290 ng cm^{-2}. This value suggested that a Vmh2 monolayer was formed, also considering the yield of the process. For further experiments, a Vmh2 concentration of 50 ng $µL^{-1}$ was used to optimize the cost efficiency of the process, achieving ≈90% of surface saturation.

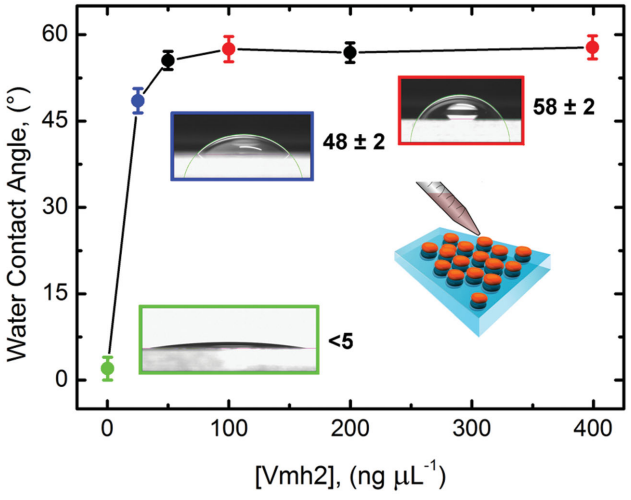

Figure 2. Optimization of superhydrophilic glass slide functionalization analyzed by WCA shift (mean ± standard deviation), which depends on Vmh2 concentration.

These results highlighted the ability of Vmh2 to self-assemble into amphiphilic monolayers efficiently modifying the wettability of surfaces. In fact, only 1 mg of Vmh2 was able to coat 100 slides (≈200 mg of Vmh2 can be extracted and purified from 1 L of fungal culture) in this process configuration. The use of ordered monolayers of hydrophobin is most probably an ideal approach for surface adhesion applications since the orientation the hydrophobin can be more easily controlled in a monolayer than in a multilayer.

Remarkably, only 4 min were needed for biofunctionalized slide fabrication, the sum of net times for plasma treatment, and the Vmh2 self-assembling process. The electrostatic interaction between Vmh2 and the negatively charged glass surface, enhanced in lower polar solvent with respect to water, could play a key role in this rapid functionalization both increasing the local concentration of Vmh2 at the solid–liquid interface and driving the orientation of the amphiphilic hydrophobin molecules to form a highly ordered amphiphilic layer.

The proposed glass biofunctionalization was fast in comparison to standard chemical processes (≈13 h) and to rapid methods for fabrication of microarray substrates.[56] Therefore, it was tested for nanomaterial and protein micropatterning/immobilization.

Third, CdTe quantum dots and proteins were patterned by a microarray robot using a protocol originally reported for antibodies printing.[7] The glass slides were masked using a multiwell microarray cassette to separate the surface in 24 chambers (see Figure S1 in the Supporting Information). In each chamber, a block of up to 550 micrometric drops can be dispensed. Alternatively, up to 16 969 drops per slide can be dispensed in an ordered array of 71 columns and 239 rows in absence of mask. Another nanomaterial, GO, was deposited in a film-like arrangement. In this case, a second homogeneous layer was assembled on the Vmh2 substrate and used for further protein patterning. In any case, the functionalized surfaces were strongly washed in the presence of detergents, particularly Tween 20 at 0.05%, to test the stability of binding. Analysis of the results obtained by proteins, QDs, and GO immobilization is described in the following sections.

2.2. Protein Immobilization

Vmh2–glass was tested for protein immobilization, and compared with a commercially available aminosilane substrate as high-performance reference substrate for immobilization of antibodies.[79] To evaluate protein adsorption and biofunctionality, two proteins, the fluorescent Alexa555–BSA conjugate (A555B) and anti-immunoglobulin (IgG) antibodies (αIgG) dissolved in aqueous buffer, were micropatterned in microarray format as previously described,[7] and, upon adsorption onto the Vmh2 substrate, washed with detergent solutions to test the binding stability. Morphology of immobilized A555B protein spots, signal to background, and coefficient of variation (CV) of fluorescence intensity were evaluated (see **Figure 3**A).

Following the incubation of 750 µg mL^{-1} A555B (the effect of different A555B concentrations is shown in Figure S2 in the Supporting Information) and harsh washing by phosphate buffered saline (PBS) supplemented with Tween 20 at 0.05% (v/v)

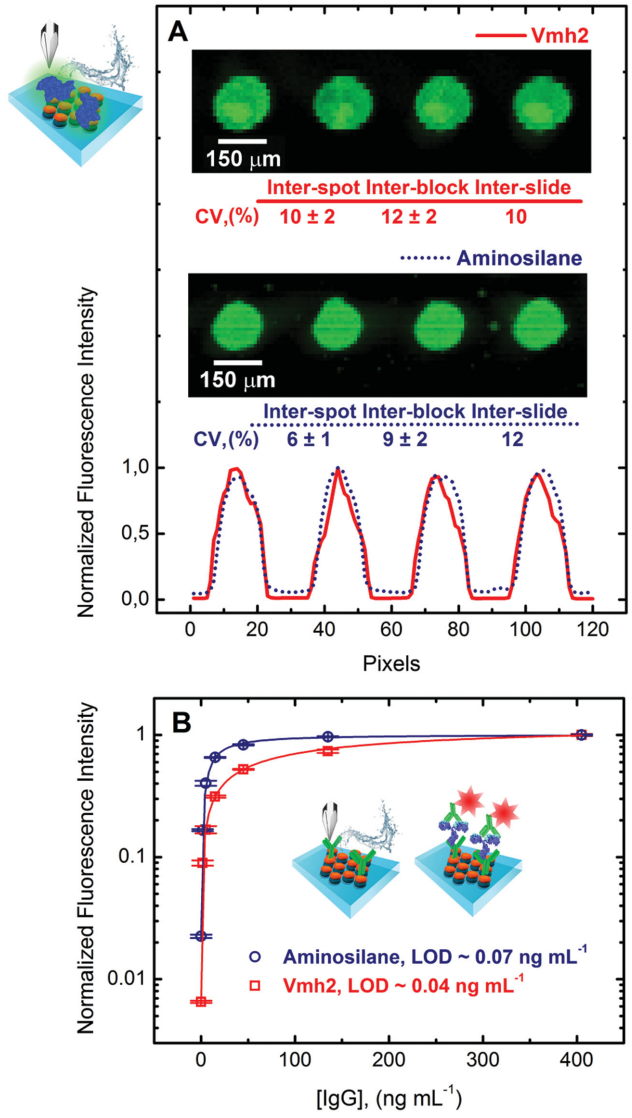

Figure 3. Micropatterning of proteins on Vmh2 hydrophobin-coated glass slides. A) Spot morphology and profile of micropatterned A555B (excited at 532 nm) on both Vmh2-coated glass slides MI (750 μg mL^{-1} A555B, 600 PMT gain laser scanner detector) and aminosilane substrate (200 μg mL^{-1} A555B, 500 PMT gain laser scanner detector), after washing by PBST. Inter-spot (n = 180 spots), inter-block (n = 18 blocks), and inter-slide (n = 3 slides) CVs are indicated (details as given in the text). B) IgG detection in a microarray format. Comparison of aminosilane with Vmh2-coated slides. Bars are representing the standard deviation of normalized fluorescence intensity (details as given in the Experimental Section). Detection curves are extrapolated by logistic fitting.

(PBST), fluorescence images of Vmh2–glass surface showed stably immobilized, circularly shaped spots, ≈75 μm radius. Moreover, the profile of fluorescence intensity (calculated over the surface area shown in the boxes, see Figure 3A), evidenced a very high signal-to-background ratio when compared with the aminosilane standard. Notably, the very low background noise confirmed the suitability of the surface functionalization by Vmh2 for optical applications, as previously tested.[67] On the other hand, aminosilane exhibited higher binding affinity (A555B was incubated at 200 μg mL^{-1} to reduce background noise), which resulted in a more homogeneous distribution of protein inside a spot, as evidenced by the intensity profile. Additionally, the effect of the plasma pretreatment was tested on the two glasses, MI and MII (see Figures S2–S4, Supporting Information), showing that it effectively improves the signal to background indifferently from the type of glass used.

The consistency of the Vmh2 coating over the whole slide was evaluated comparing the CV of 180 spots intensities with the standard aminosilane substrate. A total number of 18 blocks per slide were printed, each block made of 10 spots for a total of 180 spots per slide in triplicate experiments (see the Experimental Section for details of the statistical comparison). In this configuration, inter-spot (spot-to-spot), inter-block (block-to-block), and inter-slide (slide-to-slide) CV evidenced quite low signal variability on Vmh2 substrate (see Figure 3A).

Further characterization was aimed at evaluating the biological function of the immobilized αIgG antibodies onto the Vmh2-coated glass slides for microarray applications in optical sensing. Incubation of αIgG was performed at the same concentration (500 μg mL^{-1}) on both Vmh2 and aminosilane substrates.

Biological matrixes contain a myriad of biomolecules which could trigger an increase of background signal due to nonspecific binding of such biomolecules. When particular biological matrixes are assayed, blocking buffers of different compositions could be used to minimize the background caused by the aforementioned nonspecific binding events. Herein, prior to examination in a biological assay, a heterogeneous biological matrix (milk contained in blocking buffer, see details in the Experimental Section) was typically incubated on the functionalized surface to saturate nonspecific binding sites, minimizing the ability of the surface to adsorb interfering biomolecules.

Then IgG detection was carried out according to the previously reported method[7] in a microarray format (see Figure 3B). Analysis of calibration curves showed that the Vmh2-coated slides, even 45 d after fabrication (see Figure S5 in the Supporting Information), were comparable to the commercial standard.

2.3. QDs Immobilization

In parallel to the successful use of organic synthesis for the preparation of QDs with complex core/shell structures, the aqueous route is a relatively cheaper and less toxic process.[80–82] Carboxylated CdTe QD nanocrystals were synthesized in our laboratory (see Figures S8–S10, Supporting Information) using a water phase route in the presence of surface stabilizers. Particles showed spherical shape, 4.28 ± 1.94 (mean ± standard deviation) diameter, light absorption from UV to visible, and a single fluorescence peak centered at 660 nm (see Figure S11 in the Supporting Information).

Immobilization of QDs on the Vmh2–glass surface was performed as for proteins. Micrometric drops of 10 × 10^{-6} M QDs dissolved in spotting buffer were patterned by the robot on the Vmh2 and aminosilane substrates, incubated overnight, and the surfaces were strongly washed by detergent-containing buffer. Fluorescence images of the slides' surface were acquired

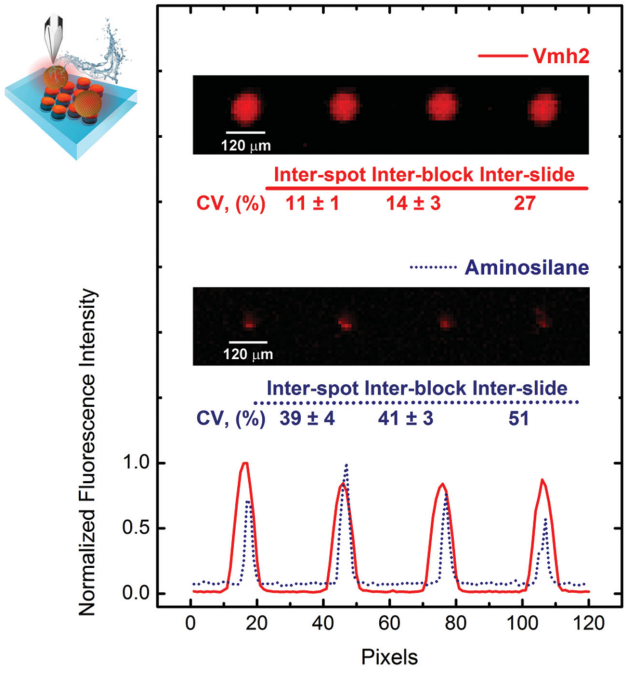

Figure 4. Micropatterning of quantum dots on Vmh2 hydrophobin-coated glass slides. Spot morphology and profile of micropatterned CdTe QDs (excited at 635 nm) on both Vmh2-coated slides and aminosilane glass slides (900 PMT), after washing by PBS–0.05% Tween 20. Inter-spot (180 spots), inter-block (18 blocks), and inter-slide (3 slides) coefficients of variation are indicated (details as given in the text).

by laser scanner (excitation 635 nm/emission 675 nm) and analyzed to evaluate QDs' immobilization (see **Figure 4**).

Micrometric spots, ≈60×10^{-6} M radius, with excellent signal to background were stably adsorbed only on the Vmh2 substrate, whereas only traces of QDs were immobilized on aminosilane. Moreover, inter-spot, inter-block, and inter-slide CV evidenced that a quite good reproducibility of immobilized spots was achieved on the Vmh2 substrate. It is worth noting that nonoptimal excitation wavelength was used, constrained by the instrument coupled light emission filter. Nevertheless, by using a 90% photomultiplier gain, very good signal to background was obtained when compared with the aminosilane substrate (see Figure 4).

2.4. Graphene Oxide Immobilization

Water-based dispersions of single-layer GO microsheets, with lateral dimensions ranging from 0.18 to 1.2 μm and showing a C/O ratio of around 1:1 (manufacturer's data, approximate values), were casted onto the surface of Vmh2-coated glass slides, incubated for 10 min at different concentrations, 0–0.8 mg mL^{-1}, washed 5 min in Milli-Q water, and dried in a stream of nitrogen. Since the GO particles are hydrophilic due to their oxygen-containing groups, the analysis of surface wettability offered a first insight into the immobilization extent (see **Figure 5**A,B). Water drops showed both high reliable contact angles over the surface of the GO–Vmh2–glass and increased hydrophilicity as a function of the GO concentration.

On the one hand, GO is an attractive substrate for efficient immobilization of active proteins, by direct adsorption on the large 2D surface functionalized with various oxygen-containing moieties.[27,83,84] On the other hand, GO is an excellent quencher of fluorescence; consequently, the GO–Vmh2–glass surface was printed with the fluorescent bovine serum albumin (BSA) spots as previously described spanning the protein, 7.5–750 μg mL^{-1} A555B, and GO concentration so as to further investigate the immobilization properties of the proposed substrate (Figure 5B). At the highest protein concentration, efficient quenching was obtained upon incubation with 0.4 mg mL^{-1} GO, as evaluated by the quantization of residual fluorescence (Figure 5A). Moreover, the wettability of the hybrid surface was appropriate for microarray patterning, even at the highest GO concentration tested (Figure 5B).

GO–Vmh2 functionalized glass slides appeared transparent to the naked eye (Figure 5D). Raman spectroscopy is a powerful technique for the analysis of graphene-related materials and their hybrid derivatives since scattering response can be observed even from one single sheet of graphene. Therefore, Raman analysis was used to compare GO binding efficiency on bare glass, aminosilane, and Vmh2-coated slides. High reproducible spectra (not normalized) were recorded in multiple positions of the Vmh2 (Figure 5C) and aminosilane (Figure S6, Supporting Information) glass surfaces, showing the characteristic D (≈1340 cm^{-1}), G (≈1600 cm^{-1}), 2D (≈2680 cm^{-1}), D+G (≈2940 cm^{-1}), and 2G (≈3180 cm^{-1}) bands.[85] Conversely, when GO was tentatively immobilized on the bare glass slides, almost no Raman signal was detected (Figure 5C). The stability of GO–Vmh2 layer was also tested. Raman analysis showed that the homogeneous layer was stably bound to Vmh2 substrate, even after vigorous washing, three times by PBST (Figure S7, Supporting Information).

Direct observation of the molecular assemblies was performed by AFM imaging in air. Due to the glass roughness, mica was chosen as molecularly flat highly hydrophilic surface for Vmh2 self-assembling. Mica sheets, freshly cleaved by adhesive tape, were coated with 400 ng cm^{-2} Vmh2, and directly dried in a stream of nitrogen. Upon incubation with 0.4 mg mL^{-1} GO, the surface was washed three times for 2 min in Milli-Q water and dried. AFM images showed that a homogeneous layer of arranged GO sheets was spontaneously self-assembled on Vmh2 substrate (Figure 5E).

3. Conclusions

The Class I hydrophobin Vmh2, extracted from the fungus *P. ostreatus*, self-assembles onto superhydrophilic glasses building highly homogeneous, transparent, and insoluble films in 2 min. One milligram of Vmh2 can functionalize an extremely large surface area of glass such as 1880 cm^2. It can be estimated that the surface is coated by a protein monolayer, which is a helpful strategy to control the orientation of the amphiphilic molecules and, therefore, its binding properties to the immobilized molecules and nanomaterials. The Vmh2 substrate tunes the surface hydrophilicity (WCA 0°–60°) and shows "adhesive" properties allowing homogeneous immobilization of micropatterned quantum dots and functional proteins or of a homogeneous second layer made of graphene oxide by

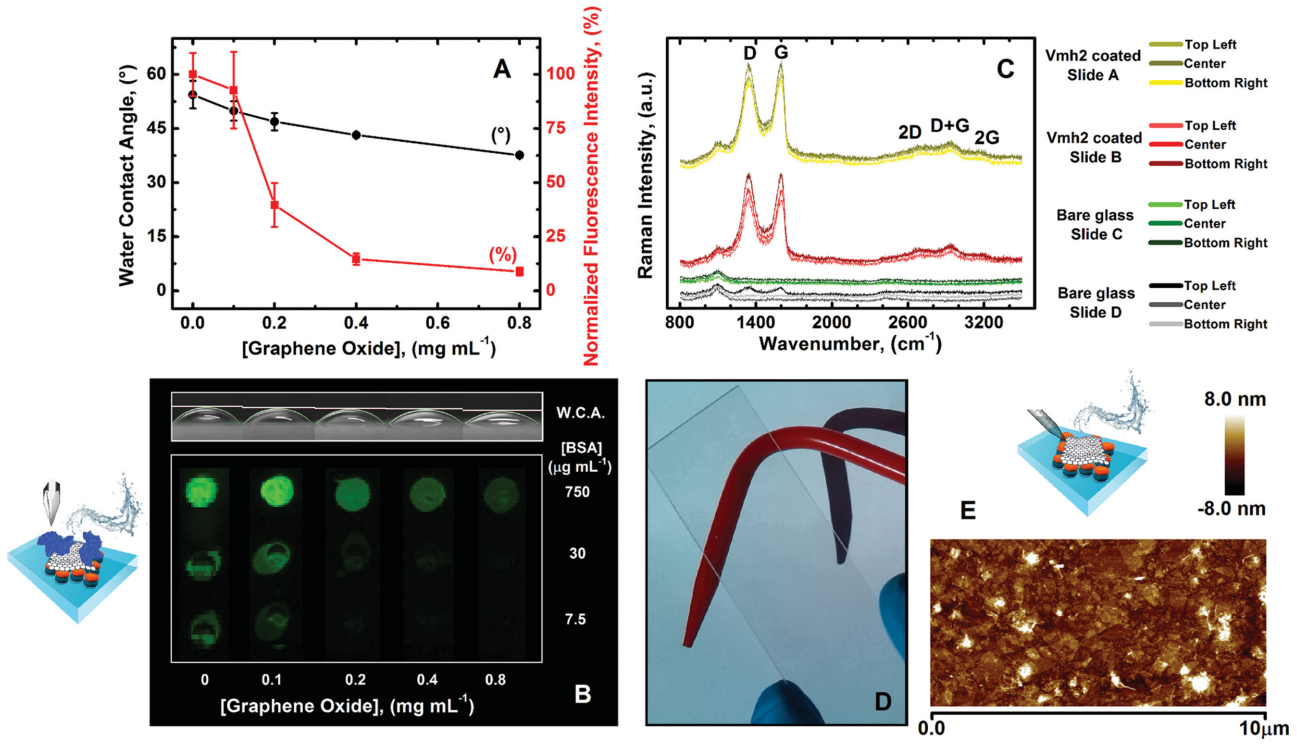

Figure 5. Immobilization of graphene oxide on Vmh2 hydrophobin-coated glass slides. A) Optimization of GO immobilization carried out by monitoring surface properties relevant to microarray technology such as water contact angle and fluorescence intensity of A555B spots (750 μg mL^{-1}). B) Same as panel (A) with spot morphology using different A555B concentrations and the picture of water drops on functionalized glass. C) Raman spectra (raw data) of Vmh2-coated slides or bare glass slides incubated with 0.4 mg mL^{-1} graphene oxide and extensively washed with water. D) Appearance of a transparent glass slide functionalized by Vmh2 and GO. E) AFM image of a GO layer on Vmh2 functionalized MICA support and a schematic representation of functionalized glass slides.

spontaneous adsorption. The molecular assemblies are stably immobilized onto the Vmh2 substrate even after harsh washes by detergent-containing solutions. It is likely that the Vmh2 layer exposes assorted chemical functionalities besides the hydrophobic patches, which allow the interaction with the heterogeneous functional groups of immobilized proteins (acid, basic, and polar and hydrophobic aminoacids) and of both QDs (carboxyl groups) and GO (various oxygen-containing groups and hydrophobic islands).[86]

This novel glass substrate is also proven to be amenable for optical biosensing applications in the microarray format, showing comparable performances with the standard aminosilane substrate in a sandwich immunoassay and low background fluorescence upon laser excitation at 533 and 635 nm. Moreover, interfacing nanomaterials and proteins on this new nanoenabled support could provide advanced bioanalytical tools,[50] and its use could be expanded to the study of nanomaterial–cell interactions.[1–3,30,54,87,88] The proposed glass nanobiofunctionalization is easily scalable through the latest reported techniques,[56] quick, and environmental friendly allowing a cost-effective modification.

4. Experimental Section

Extraction of Vmh2 from the Mycelium of P. ostreatus: White-rot fungus, *P. ostreatus* (Jacq.: Fr.) Kummer (type: Florida; ATCC No. MYA-2306) was maintained at 4 °C through periodic transfer on potato dextrose agar, Difco (BD Diagnostic Systems; Sparks, MD, USA) plates in the presence of 0.5% yeast extract, Bacto (BD Diagnostic Systems; Sparks, MD, USA). Mycelia were inoculated in 1 L flasks containing 500 mL of potato dextrose broth (24 g L^{-1}) supplemented with 0.5% yeast extract, grown at 28 °C in shaken mode (150 rpm). After 10 d of fungal growth, mycelia were separated by filtration through gauze, treated twice with 2% SDS in a boiling water bath for 10 min, washed several times with water and once with 60% ethanol to completely remove the detergent. The residue was dried under nitrogen, grinded, and treated with 100% trifluoroacetic acid (TFA) in an Elmasonic S30 water bath sonicator (Elma; Singen, Germany) for 30 min, and centrifuged (10 min at 3200 g). The supernatant was dried and then lipids were extracted in a mixture of water–methanol–chloroform 2:2:1 v/v (5 min in the bath sonicator). After centrifugation, proteins appeared as a solid aggregate at the interface between the water–methanol and the chloroform phases. They were recovered by liquid phase removal. The aggregated protein was dried, treated with TFA for 30 min in the bath sonicator, redried, and dissolved in 80% ethanol. The sample was centrifuged (90 min at 12 000 *g*) and ethanol was removed from the supernatant under vacuum at 40 °C using a Laborota-4000 rotary evaporator (Heidolph; Schwabach, Germany), and the material was freeze-dried, treated with TFA as above described and redissolved in 60% ethanol.

Plasma Treatment of Glass Slides: Precleaned plain glass slides, MI and MII, 75 × 25 mm, were purchased from two different manufactures: Corning (Corning, NY, USA) and J. Melvin Freed (Perkasie, PA, USA), respectively. MI and MII were washed by isopropanol, dried in a steam of nitrogen, and treated for 2 min by air plasma, using a PDC-002 plasma cleaner (Harrick Plasma; Ithaca, NY, USA) 29.2 W radio frequency power, equipped with a RV3F vacuum pump (Edwards; Crawley, UK).

Microarray Reagents and Solutions: Glycerol, PBS, Tween 20, and milk powder were purchased from Sigma-Aldrich (Taufkirchen, Germany). Albumin from bovine serum Alexa Fluor 555 conjugate was purchased

from Thermo Fisher Scientific (Waltham, MA, USA). Anti-IgG antibody and biotinylated detection antibody against IgG were acquired from Abcam (Milton, Cambridge, UK). Streptavidin–Alexa 647 was obtained from Invitrogen (Carlsbad, CA, USA). PBS with 2% (v/v) glycerol was used as spotting buffer. PBS supplemented with 5% (w/v) milk powder and 0.005% (v/v) Tween 20 was prepared as blocking buffer. PBS supplemented with Tween 20 at 0.05% (v/v) was used as washing buffer (PBST). PBS with 0.5% (v/v) Tween 20 containing 1% of BSA fraction V (w/v) was employed as immunobuffer. Water used to prepare the solutions was Milli-Q. Water-based dispersions of GO were purchased from Angstron Materials Inc. (Dayton, OH, USA). Quantum dot nanocrystals were synthesized and characterized in the laboratories (details as given in the Supporting Information).

Fabrication of the Antibody, A555B, and QD Microarrays: The capture anti-IgG antibody was spotted at 500 μg mL^{-1} and CdTe QDs at 10×10^{-6} M, over the Vmh2-coated glass or aminosilane glass slides (PolyAn; Berlin, Germany), in spotting buffer using Microgrid II robot (Digilab; Marlborough, MA, USA). A555B was spotted at 750 μg mL^{-1} and 200 μg mL^{-1} on the Vmh2 and aminosilane substrates, respectively. Spotting was done at room temperature and at 40%–60% humidity. The average diameter of the printed spots was ≈150 μm for proteins and 120 for QDs. After spotting, the slides were incubated at 4 °C overnight in a desiccated environment. The microarray slides were masked and divided by wells through a microarray cassette (Arrayit; Sunnyvale, CA, USA), and each well was washed three times with PBST (150 μL).

Microarray Slides Quantification: The slides were examined through an AlphaScan microarray scanner 3.0 (Alpha Innotech Corporation; San Leandro, CA, USA) using two different excitation-laser/emission-filter combinations (533exc/570em, or 635exc/670em, wavelength in nm units), depending on the explored fluorophore/photoluminescent nanomaterial, and 10 μm resolution (lengths of pixel sides). Fluorescence images of slides were obtained and explored using the AlphaScan 3.0 application software and the signal-to-background profile was measured using GenePix Pro 6.0 (Molecular Devices; Silicon Valley, CA, USA). The fluorescence intensities of spots were estimated by measuring the mean intensities of all the pixels inside the area of the spot minus the median value of pixel intensities in the local background, excluding 3 pixels of the neutral zone surrounding these spots. The fluorescence intensities of blocks (10 spots per block) were estimated by measuring the mean spots intensities, excluding the scattered point spots (spots in the first and fourth quartiles); the same spots were used for the estimation of CV. The fluorescence intensities over of whole slides (180 spots per slides printed in 18 blocks) were estimated by measuring the mean spots intensities, excluding high scattered spots (spots in the 1–10 percentile and in the 90–100 percentile); the same spots were used for the estimation of the CV.

Sandwich Immunoassay Microarray: According to the previous work,[7] the surface of slides with immobilized capture anti-IgG antibodies was saturated for 30 min with 100 μL blocking buffer. Subsequently, the masked slides were washed with PBST (100 μL per well, five times) and the microarrays were incubated for 2 h with solutions of IgG analyte in immunobuffer (100 μL per well) at different concentrations (167–400 ng mL^{-1}). The masked slides were washed with PBST (150 μL per well, five times), incubated with biotinylated detection antibody (diluted in immunobuffer at 1.5 μg mL^{-1}) for 1 h, and then rewashed with PBST (150 μL per well, seven times). The bound detection antibodies were conjugated (100 μL per well) with Streptavidin-Alexa 647 (diluted in immunobuffer at 0.4 μg mL^{-1}) for 30 min. All incubations were performed with oscillatory agitation at 300 rpm in an MTS 2/4 digital microtiter shaker (IKA; Staufen, Germany). The masked slides were washed with PBST (150 μL per well, five times), twice with PBS, and once with Milli-Q water. The slides were then unmasked, subsequently dried using a nitrogen stream and analyzed by fluorescence imaging with the aforementioned scanner. The limit of detection (LOD) of the respective calibration curve was estimated as the sum of the mean fluorescence intensity among the spots (incubated in the absence of IgG, excluding the spots in the first and fourth quartiles) and three times the standard deviation: LOD = MFI (Q2;Q3) + 3SD (Q2;Q3).

Characterization Techniques: Contact angle was measured on a DSA25B drop shape analyzer (KRÜSS; Hamburg, Germany) equipped with a CS8420Ci CCD camera (Toshiba Teli, Tokyo, Japan). Images of sessile drops of 5 μL Milli-Q water, placed in 3–5 positions of 3–10 slides, were analyzed with the software package (version 1.90.0.14, KRÜSS) using the tangent method. AFM measurements were performed on mica using a Nanoscope V Multimode8 AFM (Bruker, Germany) and Si cantilevers (SNL model, *k*: 0.3 N m^{-1}, Bruker). The scanning probe microscopy was carried out at a scan rate of 1 Hz and 512 × 512 pixel. Raman spectra were acquired using a Horiba Jobin Yvon LabRAM HR 800 (Kioto, Japan), 800mm focal length, 100× objective, and an excitation wavelength of 532 nm.

Supporting Information

Supporting Information is available from the Wiley Online Library or from the author.

Acknowledgements

A.M.G. and E.M.-N. contributed equally to this work. This work was supported by The European Commission Program, FP7-OCEAN (613844), and MINECO (Spain; BIO2013–49464-EXP and RTC-2014-2619-7); Ministero dell'Università e della Ricerca Scientifi ca (Italy), Industrial Research Project PON01_01966 EnerbioChem, funded in the frame of Operative National Programme Research and Competitiveness 2007–2013 D. D. Prot. No. 01/Ric. 18.1.2010; P.O.R. Campania FSE 2007–2013, Project CREMe. ICN2 acknowledges support from the Severo Ochoa Program (MINECO, Grant SEV-2013-0295).

Received: July 10, 2015
Revised: August 17, 2015
Published online: September 9, 2015

[1] S. M. Kang, N. S. Hwang, J. Yeom, S. Y. Park, P. B. Messersmith, I. S. Choi, R. Langer, D. G. Anderson, H. Lee, *Adv. Funct. Mater.* **2012**, *22*, 2949.
[2] V. Biju, *Chem. Soc. Rev.* **2014**, *43*, 744.
[3] C. Y. Tay, M. I. Setyawati, J. Xie, W. J. Parak, D. T. Leong, *Adv. Funct. Mater.* **2014**, *24*, 5936.
[4] I. L. Medintz, H. T. Uyeda, E. R. Goldman, H. Mattoussi, *Nat. Mater.* **2005**, *4*, 435.
[5] U. Resch-Genger, M. Grabolle, S. Cavaliere-Jaricot, R. Nitschke, T. Nann, *Nat. Methods* **2008**, *5*, 763.
[6] N. Hildebrandt, *ACS Nano* **2011**, *5*, 5286.
[7] E. Morales-Narváez, H. Montón, A. Fomicheva, A. Merkoçi, *Anal. Chem.* **2012**, *84*, 6821.
[8] S. Keuleyan, E. Lhuillier, P. Guyot-Sionnest, *J. Am. Chem. Soc.* **2011**, *133*, 16422.
[9] X. Michalet, F. F. Pinaud, L. A. Bentolila, J. M. Tsay, S. Doose, J. J. Li, G. Sundaresan, A. M. Wu, S. S. Gambhir, S. Weiss, *Science* **2005**, *307*, 538.
[10] B. A. Kairdolf, A. M. Smith, T. H. Stokes, M. D. Wang, A. N. Young, S. Nie, *Annu. Rev. Anal. Chem.* **2013**, *6*, 143.
[11] S. Marín, S. Pujals, E. Giralt, A. Merkoçi, *Bioconjug. Chem.* **2011**, *22*, 180.
[12] M. Medina-Sánchez, S. Miserere, S. Marín, G. Aragay, A. Merkoçi, *Lab Chip* **2012**, *12*, 2000.
[13] X. Wang, X. Ren, K. Kahen, M. A. Hahn, M. Rajeswaran, S. Maccagnano-Zacher, J. Silcox, G. E. Cragg, A. L. Efros, T. D. Krauss, *Nature* **2009**, *459*, 686.

[14] A. M. Smith, S. Nie, *Nat. Biotechnol.* **2009**, *27*, 732.
[15] H. Montón, C. Parolo, A. Aranda-Ramos, A. Merkoçi, C. Nogués, *Nanoscale* **2015**, *7*, 4097.
[16] S. Carregal-Romero, E. Caballero-Díaz, L. Beqa, A. M. Abdelmonem, M. Ochs, D. Hühn, B. S. Suau, M. Valcarcel, W. J. Parak, *Annu. Rev. Anal. Chem.* **2013**, *6*, 53.
[17] J. Liu, G. Li, X. Yang, K. Wang, L. Li, W. Liu, X. Shi, Y. Guo, *Anal. Chem.* **2015**, *87*, 876.
[18] R. Freeman, I. Willner, *Chem. Soc. Rev.* **2012**, *41*, 4067.
[19] V. Georgakilas, J. A. Perman, J. Tucek, R. Zboril, *Chem. Rev.* **2015**, *115*, 4744.
[20] S. Eigler, A. Hirsch, *Angew. Chem. Int. Ed. Engl.* **2014**, *53*, 7720.
[21] P. Montes-Navajas, N. G. Asenjo, R. Santamaría, R. Menéndez, A. Corma, H. García, *Langmuir* **2013**, *29*, 13443.
[22] D. Li, M. B. Müller, S. Gilje, R. B. Kaner, G. G. Wallace, *Nat. Nanotechnol.* **2008**, *3*, 101.
[23] B. J. Hong, O. C. Compton, Z. An, I. Eryazici, S. T. Nguyen, *ACS Nano* **2012**, *6*, 63.
[24] I. Chowdhury, M. C. Duch, N. D. Mansukhani, M. C. Hersam, D. Bouchard, *Environ. Sci. Technol.* **2013**, *47*, 6288.
[25] J. I. Paredes, S. Villar-Rodil, A Martínez-Alonso, J. M. D. Tascón, *Langmuir* **2008**, *24*, 10560.
[26] S. Gambhir, R. Jalili, D. L. Officer, G. G. Wallace, *NPG Asia Mater.* **2015**, *7*, e186.
[27] Y. Wang, Z. Li, J. Wang, J. Li, Y. Lin, *Trends Biotechnol.* **2011**, *29*, 205.
[28] S. S. Chou, M. De, J. Luo, V. M. Rotello, J. Huang, V. P. Dravid, *J. Am. Chem. Soc.* **2012**, *134*, 16725.
[29] B. J. Hong, Z. An, O. C. Compton, S. T. Nguyen, *Small* **2012**, *8*, 2469.
[30] P. Wick, A. E. Louw-Gaume, M. Kucki, H. F. Krug, K. Kostarelos, B. Fadeel, K. A. Dawson, A. Salvati, E. Vázquez, L. Ballerini, M. Tretiach, F. Benfenati, E. Flahaut, L. Gauthier, M. Prato, A. Bianco, *Angew. Chem. Int. Ed.* **2014**, *53*, 7714.
[31] K. P. Loh, Q. Bao, G. Eda, M. Chhowalla, *Nat. Chem.* **2010**, *2*, 1015.
[32] J. Kim, L. J. Cote, F. Kim, J. Huang, *J. Am. Chem. Soc.* **2010**, *132*, 260.
[33] T. N. Lin, L. T. Huang, G. W. Shu, C. T. Yuan, J. L. Shen, C. A. J. Lin, W. H. Chang, C. H. Chiu, D. W. Lin, C. C. Lin, H. C. Kuo, *Opt. Lett.* **2013**, *38*, 2897.
[34] L. Gaudreau, K. J. Tielrooij, G. E. D. K. Prawiroatmodjo, J. Osmond, F. J. García de Abajo, F. H. L. Koppens, *Nano Lett.* **2013**, *13*, 2030.
[35] R. S. Swathi, K. L. Sebastian, *J. Chem. Phys.* **2009**, *130*, 086101.
[36] M. Pumera, *Chem. Soc. Rev.* **2010**, *39*, 4146.
[37] K. Kostarelos, K. S. Novoselov, *Science* **2014**, *344*, 261.
[38] E. Morales-Narváez, B. Pérez-López, L. B. Pires, A. Merkoçi, *Carbon* **2012**, *50*, 2987.
[39] E. Morales-Narváez, A. Merkoçi, *Adv. Mater.* **2012**, *24*, 3298.
[40] H. Chang, H. Wu, *Adv. Funct. Mater.* **2013**, *23*, 1984.
[41] Y. Wang, L. Tang, Z. Li, Y. Lin, J. Li, *Nat. Protoc.* **2014**, *9*, 1944.
[42] S.-R. Ryoo, J. Lee, J. Yeo, H.-K. Na, Y.-K. Kim, H. Jang, J. H. Lee, S. W. Han, Y. Lee, V. N. Kim, D.-H. Min, *ACS Nano* **2013**, *7*, 5882.
[43] B. Esteban-Fernández de Ávila, A. Martín, F. Soto, M. A. Lopez-Ramirez, S. Campuzano, G. M. Vásquez-Machado, W. Gao, L. Zhang, J. Wang, *ACS Nano* **2015**, *9*, 6756.
[44] H. Jang, S.-R. Ryoo, Y.-K. Kim, S. Yoon, H. Kim, S. W. Han, B.-S. Choi, D.-E. Kim, D.-H. Min, *Angew. Chem. Int. Ed. Engl.* **2013**, *52*, 2340.
[45] L. Wang, J. Zhu, L. Han, L. Jin, C. Zhu, E. Wang, S. Dong, *ACS Nano* **2012**, *6*, 6659.
[46] H. Pei, J. Li, M. Lv, J. Wang, J. Gao, J. Lu, Y. Li, Q. Huang, J. Hu, C. Fan, *J. Am. Chem. Soc.* **2012**, *134*, 13843.
[47] H. Dong, W. Gao, F. Yan, H. Ji, H. Ju, *Anal. Chem.* **2010**, *82*, 5511.
[48] J. Li, C.-H. Lu, Q.-H. Yao, X.-L. Zhang, J.-J. Liu, H.-H. Yang, G.-N. Chen, *Biosens. Bioelectron.* **2011**, *26*, 3894.
[49] M. Li, X. Zhou, S. Guo, N. Wu, *Biosens. Bioelectron.* **2013**, *43*, 69.
[50] E. Morales-Narváez, A.-R. Hassan, A. Merkoçi, *Angew. Chem. Int. Ed. Engl.* **2013**, *52*, 13779.
[51] E. Morales-Narvaez, T. Naghdi, E. Zor, A. Merkoçi, *Anal. Chem.* **2015**, *87*, 8573.
[52] J. H. Jung, D. S. Cheon, F. Liu, K. B. Lee, T. S. Seo, *Angew. Chem. Int. Ed. Engl.* **2010**, *49*, 5708.
[53] Y. Ueno, K. Furukawa, K. Matsuo, S. Inoue, K. Hayashi, H. Hibino, *Chem. Commun.* **2013**, *49*, 10346.
[54] R. Palankar, N. Medvedev, A. Rong, M. Delcea, *ACS Nano* **2013**, *7*, 4617.
[55] P. Zuo, X. Li, D. C. Dominguez, B.-C. Ye, *Lab Chip* **2013**, *13*, 3921.
[56] J. H. Lee, H. Hyun, C. J. Cross, M. Henary, K. A. Nasr, R. Oketokoun, H. S. Choi, J. V. Frangioni, *Adv. Funct. Mater.* **2012**, *22*, 872.
[57] F. Loeffler, C. Schirwitz, J. Wagner, K. Koenig, F. Maerkle, G. Torralba, M. Hausmann, F. R. Bischoff, A. Nesterov-Mueller, F. Breitling, *Adv. Funct. Mater.* **2012**, *22*, 2503.
[58] S. Avvakumova, M. Colombo, P. Tortora, D. Prosperi, *Trends Biotechnol.* **2014**, *32*, 11.
[59] F. Han, X. Qi, L. Li, L. Bu, Y. Fu, Q. Xie, M. Guo, Y. Li, Y. Ying, S. Yao, *Adv. Funct. Mater.* **2014**, *24*, 5011.
[60] T. Sun, G. Qing, B. Su, L. Jiang, *Chem. Soc. Rev.* **2011**, *40*, 2909.
[61] Y. Lin, R. Chapman, M. M. Stevens, *Adv. Funct. Mater.* **2015**, *25*, 3183.
[62] A. Walther, A. H. E. Müller, *Chem. Rev.* **2013**, *113*, 5194.
[63] J. Bayry, V. Aimanianda, J. I. Guijarro, M. Sunde, J.-P. Latgé, *PLoS Pathog.* **2012**, *8*, e1002700.
[64] W. Wohlleben, T. Subkowski, C. Bollschweiler, B. von Vacano, Y. Liu, W. Schrepp, U. Baus, *Eur. Biophys. J.* **2010**, *39*, 457.
[65] I. Macindoe, A. H. Kwan, Q. Ren, V. K. Morris, W. Yang, J. P. Mackay, M. Sunde, *Proc. Natl. Acad. Sci. USA* **2012**, *109*, E804.
[66] V. Lo, Q. Ren, C. Pham, V. Morris, A. Kwan, M. Sunde, *Nanomaterials* **2014**, *4*, 827.
[67] L. De Stefano, I. Rea, P. Giardina, A. Armenante, I. Rendina, *Adv. Mater.* **2008**, *20*, 1529.
[68] H. A. B. Wösten, K. Scholtmeijer, *Appl. Microbiol. Biotechnol.* **2015**, *99*, 1587.
[69] S. Longobardi, A. M. Gravagnuolo, I. Rea, L. De Stefano, G. Marino, P. Giardina, *Anal. Biochem.* **2014**, *449*, 9.
[70] S. Longobardi, A. M. Gravagnuolo, R. Funari, B. Della Ventura, F. Pane, E. Galano, A. Amoresano, G. Marino, P. Giardina, *Anal. Bioanal. Chem.* **2015**, *407*, 487.
[71] A. M. Gravagnuolo, E. Morales-Narváez, S. Longobardi, E. T. da Silva, P. Giardina, A. Merkoçi, *Adv. Funct. Mater.* **2015**, *25*, 2771.
[72] S. Houmadi, F. Ciuchi, M. P. De Santo, L. De Stefano, I. Rea, P. Giardina, a Armenante, E. Lacaze, M. Giocondo, *Langmuir* **2008**, *24*, 12953.
[73] L. De Stefano, I. Rea, E. De Tommasi, I. Rendina, L. Rotiroti, M. Giocondo, S. Longobardi, a Armenante, P. Giardina, *Eur. Phys. J. E: Soft Matter* **2009**, *30*, 181.
[74] S. H. North, E. H. Lock, T. R. King, J. B. Franek, S. G. Walton, C. R. Taitt, *Anal. Chem.* **2010**, *82*, 406.
[75] E. S. Basheva, P. A. Kralchevsky, K. D. Danov, S. D. Stoyanov, T. B. J. Blijdenstein, E. G. Pelan, A. Lips, *Langmuir* **2011**, *27*, 4481.
[76] Z. Wang, M. Lienemann, M. Qiau, M. B. Linder, *Langmuir* **2010**, *26*, 8491.
[77] A. H. Y. Kwan, R. D. Winefield, M. Sunde, J. M. Matthews, R. G. Haverkamp, M. D. Templeton, J. P. Mackay, *Proc. Natl. Acad. Sci. USA* **2006**, *103*, 3621.
[78] A. Armenante, S. Longobardi, I. Rea, L. De Stefano, M. Giocondo, A. Silipo, A. Molinaro, P. Giardina, *Glycobiology* **2010**, *20*, 594.
[79] S. L. Seurynck-Servoss, A. M. White, C. L. Baird, K. D. Rodland, R. C. Zangar, *Anal. Biochem.* **2007**, *371*, 105.

[80] V. Lesnyak, N. Gaponik, A. Eychmüller, *Chem. Soc. Rev.* **2013**, *42*, 2905.
[81] Y. Li, L. Jing, R. Qiao, M. Gao, *Chem. Commun.* **2011**, *47*, 9293.
[82] J. Tian, R. Liu, Y. Zhao, Q. Xu, S. Zhao, *J. Colloid Interface Sci.* **2009**, *336*, 504.
[83] H. Xu, D. Wang, S. He, J. Li, B. Feng, P. Ma, P. Xu, S. Gao, S. Zhang, Q. Liu, J. Lu, S. Song, C. Fan, *Biosens. Bioelectron.* **2013**, *50*, 251.
[84] S. Hermanová, M. Zarevúcká, D. Bouša, M. Pumera, Z. Sofer, *Nanoscale* **2015**, *7*, 5852.
[85] A. Jorio, M. S. Dresselhaus, R. Saito, G. Dresselhaus, *Raman Spectroscopy in Graphene Related Systems*; Wiley-VCH, Weinheim, Germany **2011**.
[86] K. Erickson, R. Erni, Z. Lee, N. Alem, W. Gannett, A. Zettl, *Adv. Mater.* **2010**, *22*, 4467.
[87] P. Rivera-Gil, D. Jimenez de Aberasturi, V. Wulf, B. Pelaz, P. del Pino, Y. Zhao, J. M. de la Fuente, I. Ruiz de Larramendi, T. Rojo, X.-J. Liang, W. J. Parak, *Acc. Chem. Res.* **2013**, *46*, 743.
[88] M. Elsabahy, K. L. Wooley, *Acc. Chem. Res.* **2015**, *48*, 1620.